Chin. J. Astron. Astrophys. Vol. 7 (2007), No. 1, 63–70
(*http://www.chjaa.org*)

Chinese Journal of
Astronomy and
Astrophysics

Evidence of the Link between Broad Emission Line Regions and Accretion Disks in Active Galactic Nuclei *

Yun Xu[1,2] and Xin-Wu Cao[1]

[1] Shanghai Astronomical Observatory, Chinese Academy of Sciences, Shanghai 200030; *xuyun@shao.ac.cn*
[2] Graduate School of Chinese Academy of Sciences, Beijing 100049

Received 2006 March 17; accepted 2006 April 18

Abstract There is observational evidence that broad-line regions (BLRs) exist in most active galactic nuclei (AGNs), but their origin is still unclear. One scenario is that the BLRs originate from winds accelerated from the hot coronae of the disks, and the winds are suppressed when the black hole is accreting at low rates. This model predicts a relation between $\dot{m}$ ($\dot{m} = \dot{M}/\dot{M}_{\rm Edd}$) and the FWHM of broad emission lines. We estimate the central black hole masses for a sample of bright AGNs by using their broad H$_\beta$ line-widths and optical luminosities. The dimensionless accretion rates $\dot{m} = \dot{M}/\dot{M}_{\rm Edd}$ are derived from the optical continuum luminosities by using two different models: using an empirical relation between the bolometric luminosity $L_{\rm bol}$ and the optical luminosity ($\dot{m} = L_{\rm bol}/L_{\rm Edd}$, a fixed radiative efficiency is adopted); and calculating the optical spectra of accretion disks as a function of $\dot{m}$. We find a significant correlation between the derived $\dot{m}$ and the observed line width of H$_\beta$, FWHM$\propto \dot{m}^{-0.37}$, which almost overlaps the disk-corona model calculations, if the viscosity $\alpha \approx 0.1 - 0.2$ is adopted. Our results provide strong evidence for the physical link between the BLRs and accretion disks in AGNs.

Key words: accretion, accretion disks—galaxies: active—galaxies: theory— radiation mechanisms: emission lines— black hole physics

1 INTRODUCTION

Most bright active galactic nuclei (AGNs) exhibit broad emission lines, with full width at half maximum (FWHM $\geq 10^3$ km s^{-1}) (Peterson et al. 1999). Some type 1 AGNs could have very broad emission lines (FWHM$\geq$ 20 000 km s^{-1}). Type 2 AGNs show only narrow lines (FWHM$\leq$ 1000 km s^{-1}) and at least some of them show evidence of containing hidden type 1 AGNs (Antonucci & Miller 1985; Tran 1995; Veilleux et al. 1997; Veilleux et al. 1999). This could be explained in the frame of the unification scheme (Antonucci 1993). However, observations either in the polarized light or near-IR show that some type 2 AGNs have no obscured broad line (true type 2 AGNs). The statistical investigations on the isotropic assumption of types 1 and 2 AGNs suggest that there exists some true type 2 AGNs (Tran 2001, 2003; Gu & Huang 2002).

It is still unclear why those true type 2 AGNs lack broad emission lines. Laor (2003) suggested that a broad line region (BLR) can survive only if the bolometric luminosity of AGN is above a threshold $L_{\rm min} \sim 10^{41.8}(M_{\rm bh}/10^8 M_\odot)^2$, based on the fact that no broad line width FWHM $> 25\,000$ km s^{-1} has been observed in any AGNs. They further suggested that the formation of BLR might be related with the accretion rate. A more detailed model was suggested by Nicastro (2000). It is shown there is a threshold

* Supported by the National Natural Science Foundation of China.

value of $\dot{m}_{\rm thres} \simeq 10^{-3}$ (in Eddington units), below which non-hidden BLR sources lie, while all hidden BLR sources have $\dot{m} \geq \dot{m}_{\rm thres}$ (Nicastro et al. 2003). In this model, the origin of the broad line clouds is related with the vertical disk winds, which originated at a critical distance in the accretion disk. The broad line widths are roughly the Keplerian velocities of the accretion disk at the radius of the wind onset. Based on Nicastro's disk-corona model, where the winds could be switched off when the accretion rate is lower than a threshold value $\dot{m}_{\rm thres}$. This model naturally predicted a relation between the size of the BLR and the accretion rate $\dot{m}$, which may be tested against the observations.

In this work we use a sample of bright AGNs with black hole masses estimated from broad line widths to test this model of BLR formation. The cosmological parameters $H_0 = 70\,{\rm km\,s^{-1}Mpc^{-1}}$, $\Omega_{\rm M} = 0.3$ and $\Omega_\Lambda = 0.7$ are adopted.

2 MODEL

In this paper we mainly follow the Nicastro's model and use a sample of bright AGNs to test the model for BLRs. We first summarize their model in this section.

In the disk-corona model, the fraction of gravitational energy dissipated in the corona is (Witt et al. 1997)

$$(1-\beta) \simeq 0.034 \left(\alpha f \frac{1}{\eta}\dot{m}\right)^{-1/4} r^{3/8}, \tag{1}$$

where η is the efficiency, $f = 1-r^{-0.5}$, $m = M/M_\odot$, $\dot{m} = \dot{M}/\dot{M}_{\rm Edd}$ and $r = R/R_0$ are the dimensionless parameters. $\dot{M}_{\rm Edd} = 1.5 \times 10^{17}\eta^{-1}m\ {\rm g\ s^{-1}}$ and $R_0 = 6GM_{\rm bh}/c^2$.

For the standard thin accretion disk (Shakura & Sunyaev 1973), the transition radius, $r_{\rm\,tran}$, at which the radiation pressure equals the gas pressure, is

$$r_{\rm tran} f^{-16/21} \simeq 15.2(\alpha m)^{2/21}\left(\frac{1}{\eta}\dot{m}\right)^{16/21}. \tag{2}$$

If the accretion rate $\dot{m} < \dot{m}_{\rm min}$, then the transition radius $r_{\rm tran}$ goes to the inner radius of the disk, and the disk is stable down to the last stable orbit. In this case there is no radiation pressure dominated region in the disk, and no radiation pressure-supported and driven wind. Therefore, there is no BLR in some low-luminosity AGNs that accrete at low rates $\dot{m} < \dot{m}_{\rm min}$. When $\dot{m} > \dot{m}_{\rm min}$, the thin disk is unstable (Lightman & Eardley 1974; Shakura & Sunyaev 1976), and a stabilizing disk/corona+outflow system forms (Witt et al. 1997). The disk/corona configuration extends to $r_{\rm\,max}$, which is derived from Equation (1) by setting $\beta = 0$:

$$r_{\rm max} f^{-2/3} \simeq 8000\left(\alpha\frac{1}{\eta}\dot{m}\right)^{2/3}. \tag{3}$$

The averaged radius $r_{\rm wind}$ for the outflow/BLR can be obtained by weighting the radial distance by $(1-\beta)$, i.e., $r_{\rm wind} = \int_{r_{\rm tran}}^{r_{\rm max}} r(1-\beta)dr / \int_{r_{\rm tran}}^{r_{\rm max}} (1-\beta)dr$. The observed FWHM values of the lines emitted by the clouds originating from the coronal outflows can be calculated from the relation FWHM$= 2(\langle v^{\,2}\rangle)^{1/2}$ (Netzer 1991), where $(\langle v^2\rangle)^{1/2} = v/\sqrt{2} = ((6r_{\rm wind})^{-1/2}c/\sqrt{2})$ is the averaged Keplerian velocity in a cylindrical geometry (see Nicastro 2000 for details). Thus we can calculate the relation between accretion rate $\dot{m}$ and FWHM from Equations (2) and (3), when the value of viscosity α is specified.

3 THE SAMPLE

In this paper, we adopt the sample of X-ray selected AGNs with optical spectroscopic observations by Xu et al. (2003). The detailed sample selection criteria can be found in Wei et al. (1999). We select all AGNs in this sample with well measured FHHM of $\rm H_\beta$ lines, leading to a sample of 110 sources (see Table 1).

Table 1 Data of 110 X-ray AGNs in Seyfert 1-type AGN sample

Name	z	FWHM of H_β (km s^{-1})	$\log L_{\rm bol}$ (erg s^{-1})	$\log \dot{m}$	$\log M_{\rm bh}$ ($M_\odot$)	$\log L_{\rm B}$ erg s^{-1}	$\log r_{\rm wind}$ $6GM/c^2$
1RXS J000011.9+052318	0.0400	3050.0	44.45	–0.947	7.302	44.03	3.6904
1RXS J000055.5+172346	0.2150	6420.0	45.45	–1.295	8.646	44.77	3.0861
1RXS J000550.0+102249	0.0950	4240.0	45.18	–1.015	8.097	44.25	1.5542
1RXS J000915.0+243758	0.1180	3880.0	45.32	–0.898	8.113	44.50	2.1955
1RXS J001121.2+373919	0.1040	3770.0	44.93	–0.988	7.819	44.58	1.9109
1RXS J001452.7+270549	0.0860	3350.0	44.59	–0.990	7.475	44.38	1.9627
1RXS J002007.2+324423	0.0820	3820.0	44.75	–1.053	7.707	44.10	2.4253
1RXS J002445.3+082047	0.0670	1660.0	44.13	–0.515	6.548	43.73	1.7582
1RXS J002902.7+195717	0.2640	5720.0	45.99	–1.034	8.920	45.28	4.2147
1RXS J003221.1+242359	0.0660	3460.0	44.06	–1.175	7.136	43.85	1.4952
1RXS J004459.4+192143	0.1790	3900.0	45.69	–0.791	8.377	45.12	3.4159
1RXS J005050.6+353645	0.0580	5470.0	44.99	–1.294	8.184	44.42	1.6878
1RXS J005607.6+254802	0.1530	6600.0	45.19	–1.398	8.486	44.88	2.0205
1RXS J011655.1+254937	0.0990	4000.0	45.40	–0.898	8.201	43.93	1.8681
1RXS J011745.5+363718	0.1070	3770.0	45.74	–0.747	8.383	44.87	2.3871
1RXS J012923.0+223100	0.2310	4730.0	45.66	–0.968	8.525	45.01	2.1488
1RXS J014023.0+240255	0.0720	4620.0	44.89	–1.179	7.964	44.45	1.4672
1RXS J014025.2+382400	0.0670	3110.0	44.38	–0.987	7.266	44.44	1.6736
1RXS J015536.7+311525	0.1350	3830.0	45.19	–0.925	8.014	44.62	2.9393
1RXS J015555.6+040620	0.1360	6980.0	44.93	–1.524	8.354	44.59	2.0097
1RXS J015621.6+241838	0.1550	3770.0	45.55	–0.803	8.251	44.77	2.1019
1RXS J023601.9+082124	0.2880	4390.0	46.12	–0.763	8.785	46.20	2.6061
1RXS J024214.5+074442	0.4510	4950.0	46.34	–0.802	9.044	46.08	2.2268
1RXS J033522.6+190739	0.1890	6180.0	45.85	–1.141	8.894	45.26	1.6253
1RXS J034308.0+185836	0.1100	3420.0	45.75	–0.658	8.308	44.87	1.7038
1RXS J035147.6+103618	0.1850	5100.0	45.39	–1.112	8.405	45.71	2.0393
1RXS J041147.1+132417	0.2770	2960.0	46.66	–0.260	8.819	46.50	2.8284
1RXS J044428.6+122113	0.0890	3140.0	45.91	–0.537	8.342	44.69	1.8866
1RXS J062334.6+644542	0.0860	4400.0	44.96	–1.116	7.970	44.78	1.6982
1RXS J065136.5+563732	0.0640	2750.0	44.68	–0.789	7.371	45.12	1.8796
1RXS J071006.0+500243	0.1540	4030.0	45.85	–0.772	8.518	44.86	3.2938
1RXS J071339.7+382043	0.1230	4140.0	45.62	–0.865	8.379	44.69	1.9844
1RXS J071858.2+705920	0.0660	4810.0	44.44	–1.348	7.687	43.73	1.3001
1RXS J071923.7+570840	0.1750	6540.0	46.09	–1.121	9.106	45.19	3.1454
1RXS J072220.6+732041	0.3500	3570.0	46.02	–0.614	8.535	45.71	1.6815
1RXS J072408.4+355309	0.1380	7260.0	45.41	–1.414	8.723	45.15	1.8230
1RXS J072826.6+303407	0.1000	3980.0	44.91	–1.043	7.848	44.24	1.2827
1RXS J073308.7+455511	0.1420	8070.0	45.74	–1.406	9.048	45.22	2.7432
1RXS J074311.3+742926	0.3320	7380.0	45.99	–1.253	9.147	45.51	1.7202
1RXS J074759.2+205229	0.1560	5540.0	45.93	–1.025	8.850	44.92	1.5732
1RXS J075039.5+624205	0.1940	6300.0	44.97	–1.422	8.295	44.88	1.2044
1RXS J075910.0+115152	0.0500	4470.0	44.49	–1.270	7.655	43.74	1.4167
1RXS J080132.3+473618	0.1570	7840.0	45.77	–1.371	9.046	45.21	2.9591
1RXS J080534.6+543132	0.4060	5780.0	47.06	–0.720	9.683	46.04	2.4703
1RXS J080639.9+724831	0.1000	1760.0	45.34	–0.203	7.446	44.43	1.6294
1RXS J081502.4+525304	0.1260	4110.0	45.32	–0.946	8.169	44.70	2.8531
1RXS J081651.4+180252	0.1580	3890.0	45.12	–0.958	7.981	45.08	1.9889
1RXS J081718.6+520200	0.2830	2170.0	45.77	–0.256	7.929	43.43	2.6325
1RXS J082942.2+415442	0.1260	7960.0	44.72	–1.702	8.318	44.58	1.9451
1RXS J084026.2+033316	0.0600	4940.0	44.50	–1.352	7.753	44.07	1.4048
1RXS J084622.3+031318	0.1070	4380.0	44.85	–1.142	7.896	44.56	2.2168
1RXS J084918.7+531806	0.1120	2750.0	45.14	–0.653	7.689	44.18	2.2720
1RXS J085233.3+422539	0.1370	2670.0	44.80	–0.727	7.430	44.46	2.2446
1RXS J085358.8+770054	0.1060	5480.0	45.05	–1.277	8.228	44.39	2.6783
1RXS J085443.8+401912	0.1520	5520.0	45.22	–1.232	8.355	44.68	1.9998
1RXS J085902.0+484611	0.0830	4420.0	44.92	–1.131	7.946	44.65	1.6582
1RXS J190910.3+665222	0.1900	3830.0	45.50	–0.833	8.228	45.31	2.4724
1RXS J193929.8+700752	0.1100	4850.0	45.56	–1.020	8.476	44.98	2.2337
1RXS J212654.3+112403	0.1000	2730.0	45.23	–0.618	7.750	44.60	1.7593
1RXS J215912.7+095247	0.1000	5380.0	44.70	–1.365	7.970	44.72	2.1154
1RXS J221537.8+290239	0.2300	5980.0	46.11	–1.035	9.046	45.28	2.8800
1RXS J222537.5+225917	0.1730	2150.0	45.61	–0.298	7.805	44.63	1.4520

Table 1 Continued.

Name	z	FWHM of H_β (km s^{-1})	$\log L_{\rm bol}$ (erg s^{-1})	$\log \dot{m}$	$\log M_{\rm bh}$ ($M_\odot$)	$\log L_{\rm B}$ erg s^{-1}	$\log r_{\rm wind}$ $6GM/c^2$
1RXS J222934.3+305720	0.3200	7930.0	46.76	–1.084	9.748	45.36	3.5016
1RXS J223019.5+163114	0.0800	4270.0	45.24	–1.004	8.143	44.37	1.4914
1RXS J224939.6+110016	0.0800	4390.0	45.47	–0.958	8.331	44.47	2.2604
1RXS J225148.5+341937	0.1300	3050.0	45.24	–0.711	7.852	45.15	1.9097
1RXS J225209.6+264236	0.0690	2160.0	44.27	–0.702	6.876	44.17	1.7119
1RXS J231456.0+224325	0.1680	3750.0	46.05	–0.649	8.597	45.01	3.9303
1RXS J232554.6+215310	0.1200	5260.0	45.68	–1.053	8.634	45.30	1.9521
1RXS J234728.8+242743	0.1600	4270.0	45.44	–0.945	8.281	45.28	1.7432
1RXS J235152.7+261938	0.0400	3750.0	44.26	–1.186	7.342	44.03	1.2711
1RXS J235754.3+132418	0.1150	4290.0	45.29	–0.992	8.185	44.68	2.9352
II ZW 2	0.0900	4990.0	45.65	–1.016	8.568	45.08	2.3436
4C 25.01	0.2840	4310.0	46.68	–0.580	9.161	45.42	2.6815
PG 0026+12	0.1420	4890.0	46.03	–0.884	8.817	45.41	1.6344
S 10785	0.1340	5970.0	45.51	–1.214	8.624	45.15	1.6126
MARK 1148	0.0640	5560.0	45.04	–1.294	8.232	44.68	1.4755
PG 0052+251	0.1550	5110.0	46.07	–0.912	8.879	45.47	2.5872
B2 0110+29	0.3630	7360.0	46.37	–1.138	9.408	45.42	2.152
3C 48.0	0.3670	4080.0	46.70	–0.525	9.129	46.46	1.8569
MS 02448+1928	0.1760	4510.0	45.81	–0.881	8.590	45.14	1.5100
MS 03574+1046	0.1820	4160.0	46.02	–0.748	8.665	45.91	2.1939
MS 07007+6338	0.1520	5070.0	45.95	–0.939	8.793	44.92	2.0751
VII ZW 118	0.0790	4910.0	45.78	–0.964	8.640	45.14	1.8228
F 07144+4410	0.0610	3820.0	45.23	–0.911	8.038	44.88	1.5905
MS 07199+7100	0.1250	4020.0	45.19	–0.967	8.056	44.57	2.1670
RX J07491+2842	0.3440	4710.0	46.25	–0.785	8.938	45.33	2.8933
RX J07527+2617	0.0820	2940.0	43.99	–1.056	6.942	44.43	1.4248
B3 0754+394	0.0960	3840.0	46.07	–0.664	8.629	44.32	3.8762
KUV 07549+4228	0.2100	4620.0	45.75	–0.920	8.568	45.33	1.9669
PG 0804+761	0.1000	5490.0	45.72	–1.077	8.701	45.31	2.0110
RX J08297+3252	0.1270	3420.0	45.05	–0.868	7.818	44.33	1.4064
RX J08307+3405	0.0630	4500.0	44.53	–1.264	7.689	44.06	1.9213

4 BLACK HOLE MASS

Kaspi et al. (2000) derived an empirical relation between the BLR size measured with the reverberation mapping method (Peterson 1993) and the optical continuum luminosity for a sample of Seyfert 1 galaxies and quasars (assuming the cosmological parameters $H_0 = 75\ {\rm km\ s^{-1}\ Mpc^{-1}}$ and $q_0 = 0.5$). The relation

$$R_{\rm BLR} = 26.4(\pm 3.0)\left[\frac{\lambda L_\lambda(5100{\rm \AA})}{10^{44}{\rm erg\ s^{-1}}}\right]^{0.610\pm0.10} \quad {\rm lt-days} \tag{4}$$

is derived by McLure & Jarvis(2002) for the same sample, but for the same cosmological parameters as used here: $\Omega_{\rm M} = 0.3$, $\Omega_\Lambda = 0.7$ and $H_0 = 70\ {\rm km\ s^{-1}\ Mpc^{-1}}$.

The central black hole masses $M_{\rm bh}$ can be estimated from the velocities $v_{\rm BLR}$ of the clouds in the BLRs

$$M_{\rm bh} = \frac{v_{\rm BLR}^2 R_{\rm BLR}}{G}, \tag{5}$$

where the motions of the clouds are assumed to be virialized and isotropic. The velocities of the clouds in the BLRs, $v_{\rm BLR}$, are derived from the widths of the broad emission lines.

5 ACCRETION RATE

5.1 Method - 1

For normal bright quasars, the bolometric luminosity can be estimated from the optical luminosity $L_{\lambda,{\rm opt}}$ at 5100 Å by Kaspi et al. (2000)

$$L_{\rm bol} \simeq 9\lambda L_{\lambda,{\rm opt}}\,. \tag{6}$$

The optical luminosity $L_{\lambda,\rm opt}$ at 5100 Å is derived from the B-band magnitude on adopting spectral index $\alpha_{\rm o}$ ($f_\nu \propto \nu^{-\alpha_{\rm o}}$) given by Xu et al. (2003). Assuming a fixed accretion efficiency for all quasars, we have the conventionally defined dimensionless accretion rate,

$$\dot{m} = \frac{L_{\rm bol}}{L_{\rm Edd}} \,. \tag{7}$$

The accuracy of the dimensionless accretion rate derived in this way mainly depends on the empirical relation (6), from which some individual sources may deviate to some degree.

5.2 Method - 2

In this work we adopt an alternative approach to estimate the accretion rate. As the disk-corona model described in Section 2, we can calculate the flux due to viscous dissipation in the cold disk by

$$F_{\rm vis}(R) \simeq \frac{3GM_{\rm bh}\dot{M}}{8\pi R^3}\beta f \,. \tag{8}$$

The local disk temperature of the thin cold disk is

$$T_{\rm disk}(R) = \frac{F_{\rm vis}(R)^{1/4}}{\sigma_{\rm B}^{1/4}} \,, \tag{9}$$

by assuming local blackbody emission. The optical emission of the disk-corona system is mainly from the cold disk. Then the B-band luminosity of cold accretion disk can be calculated by

$$\nu L_\nu^{\rm B} = 8\pi^2 \left(\frac{GM}{c^2}\right)^2 \frac{h\nu^3}{c^2} \int_1^{r_{\rm max}} \frac{rdr}{f_{\rm col}^4 \exp(h\nu/f_{\rm col}k_B T_{\rm disk}) - 1} \,, \tag{10}$$

where $\nu = 6.818 \times 10^{14}$ Hz. The correction $f_{\rm col}$ has the form (Chiang 2002)

$$f_{\rm col}(T_{\rm disk}) = f_\infty - \frac{(f_\infty - 1)[1 + \exp(-\nu_{\rm b}/\Delta\nu)]}{1 + \exp[(\nu_{\rm p} - \nu_{\rm b})/\Delta\nu]}, \tag{11}$$

where $\nu_{\rm p} = 2.82\, k_B T_{\rm disk}/h$ is the peak frequency of a blackbody with temperature $T_{\rm disk}$. This expression for $f_{\rm col}$ goes from unity at low temperature to f_∞ at high temperature with a transition at $\nu_{\rm b} \approx \nu_{\rm p}$. Chiang (2002) found that $f_\infty = 2.3$ and $\nu_{\rm b} = \Delta\nu = 5 \times 10^{15}$ Hz would do a reasonable job of reproducing the model disk spectra of Hubeny et al. (2001).

The optical continuum luminosity $L_{\rm B}$ can be calculated by using Equations (8)–(11) for a given black hole mass $M_{\rm bh}$ and accretion rate $\dot{m}$. In this way, the accretion rate $\dot{m}$ can be estimated from the observed optical continuum luminosity $L_{\rm B}$, if the black hole mass $M_{\rm bh}$ is known.

6 RESULTS

As described in Section 4 we can estimate the black hole masses of the sources in this sample from their $\rm H_\beta$ line widths and optical continuum luminosities. In Figure 1 we plot the relation between $\dot{m}$ and FWHM for the whole sample. In this figure we adopt the method-1 described in Section 5 to estimate the accretion rates $\dot{m}$ for all sources, i.e., using the empirical relation (6) for a fixed radiative efficiency. A correlation between $\dot{m}$ and FWHM is found at a significant level $> 99.99\%$. The linear regression gives

$$\log_{10} {\rm FWHM} = -0.375 \log_{10} \dot{m} + 3.327 \,. \tag{12}$$

We select sources with black hole masses $\sim 10^8 - 10^9 M_\odot$ (sources between the two vertical lines in Fig. 4), and find that significant level for the correlation between $\dot{m}$ and FWHM is again $> 99.99\%$. The linear regression gives

$$\log_{10} {\rm FWHM} = -0.337 \log_{10} \dot{m} + 3.338 \,. \tag{13}$$

We note that the derived accretion rates $\dot{m}$ depends sensitively on the value of the FWHM. We will come back to this issue in Section 7 to show why this correlation is intrinsic, and is not caused by the common

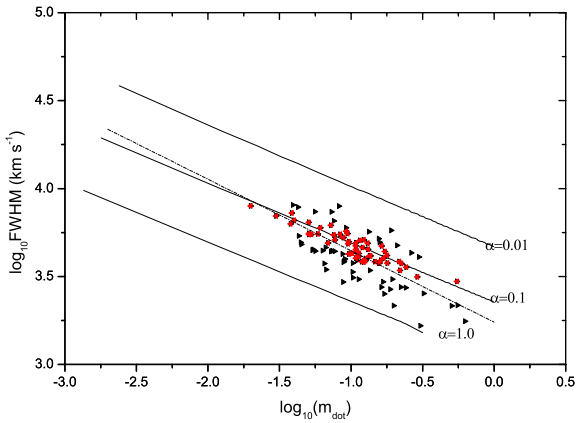

Fig. 1 Correlation between accretion rate $\dot{m}$ and FWHM. Triangles represent sources of the sample and hexagons those with $M_{\rm bh} \sim 10^8 - 10^9\ M_\odot$. The solid lines represent the model calculations for $\alpha = 0.01$, 0.1 and 1. The dash-dotted line is the linear regression line of the data.

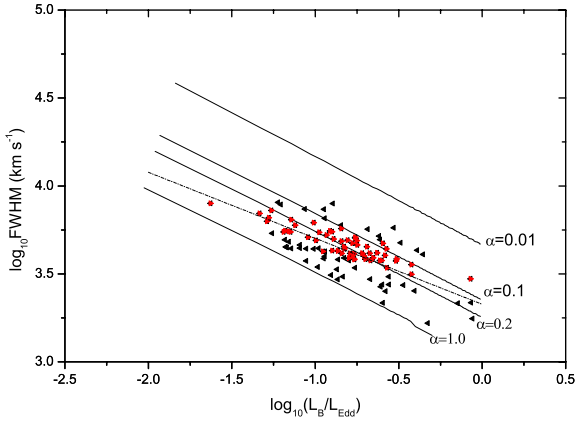

Fig. 2 Correlation between the ratio $L_{\rm B}/L_{\rm Edd}$ and FWHM. Triangles represent sources of the sample and hexagons those with $M_{\rm bh} \sim 10^8 - 10^9 M_\odot$. The solid lines represent the model calculations for α=0.01, 0.1, 0.2 and 1. The dash-dotted line is the linear regression line of the data.

dependence on FWHM. For a given black hole mass $M_{\rm bh}$ we can calculate the relation between $\dot{m}$ and FWHM using the method described in Section 2, if the viscosity α is specified. In this work, we adopt $M_{\rm bh} = 10^9 M_\odot$ in all our model calculations. We note that the results are insensitive to the black hole mass, if the black hole mass varies by one or two orders of magnitude (see Eq. (2), and Nicastro 2000). So, this simplification will not affect our main results, since most sources in our sample have black hole masses around $10^8 - 10^9\ M_\odot$ (see Table 1).

The results predicted by the model are also plotted in Figure 1. It is found that the theoretical model calculations can reproduce almost the same result as the linear regression, if $\alpha = 0.1$ is adopted in the calculations.

As discussed in Section 5.2, the dimensionless accretion rate $\dot{m}$ can be estimated from the optical continuum luminosity $L_{\rm B}$ based on the spectral calculation for the disk-corona system. In Figure 2 we plot the relation between $L_{\rm bol}/L_{\rm Edd}$ and FWHM. To compare with Figure 1 we adopt the quantity $L_{\rm bol}/L_{\rm Edd}$

instead of $\dot{m}$ in Figure 2. The values of FWHM and $L_{\rm bol}/L_{\rm Edd}$ can be calculated simultaneously by using the formalism presented in Sections 2 and 5.2 as different functions of $\dot{m}$, if the black hole mass $M_{\rm bh}$ is specified. The relation between $L_{\rm bol}/L_{\rm Edd}$ and FWHM predicted by this disk-corona model can be obtained from the model calculations by varying $\dot{m}$ for different values of viscosity parameter α. Here $M_{\rm bh} = 10^9 M_\odot$ is adopted for Figure 2. We find that the results are quite similar to those in Figure 1. The theoretical model calculations can almost reproduce the linear regression for the sample, if $\alpha = 0.2$ is adopted (see Fig. 2).

7 DISCUSSION

We find a significant correlation between $\dot{m}$ and the FWHM of broad line $\rm H_\beta$. The black hole mass $M_{\rm bh}$ is derived from the FHWH and the optical continuum luminosity (see Eqs. (4) and (5)), so that the derived black hole mass depends on the FWHM to some extent. One may worry whether it may affect the present correlation. We have plotted the correlation between $M_{\rm bh}$ and $\dot{m}$ in Figure 3, and no correlation is found between these two quantities for the whole sample. We also plot the correlation between $M_{\rm bh}$ and FWHM in Figure 4, and neither is a correlation found between the two quantities for the sources with $M_{\rm bh} \sim 10^8 - 10^9 M_\odot$. In Figure 1, however, we find that FWHM is still well correlated with $\dot{m}$ for these sources represented by hexagons. These results indicate that the correlation between $\dot{m}$ and FWHM in this work is indeed intrinsic, and is not caused by the dependence on FWHM when deriving $\dot{m}$. A similar correlation was reported by Warner et al. (2004) for a large AGN sample (see fig. 5 in their paper).

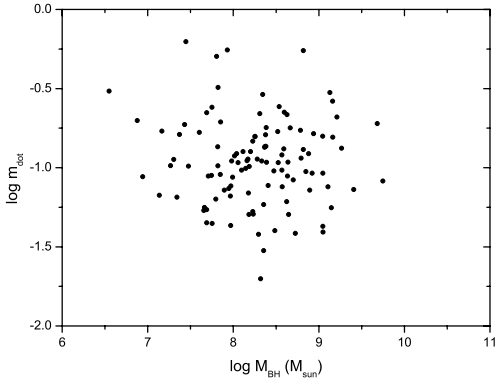

Fig. 3 Correlation between $M_{\rm bh}$ and $\dot{m}$ of the sources in the sample.

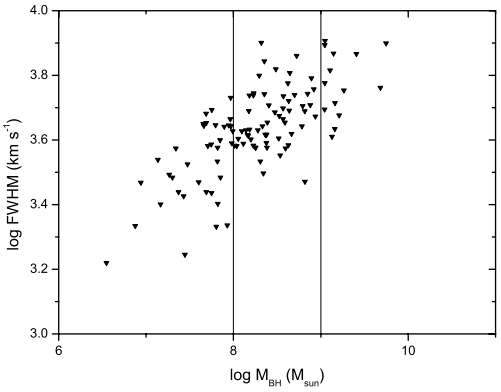

Fig. 4 Correlation between $M_{\rm bh}$ and FWHM of the sources in the sample.

The "disk/corona+outflow" model suggested by Nicastro (2000) for the BLRs in AGNs can successfully explain why some low-luminosity AGNs have no BLRs. This model suggests that the origin of BLRs is regulated by the accretion rate $\dot{m}$. The correlation between $\dot{m}$ and FWHM (or $L_{\rm bol}/L_{\rm Edd}$ and FWHM in Fig. 2) found in this work is almost same as the model prediction, which seems to support Nicastro's scenario for BLR formation. Our further calculations based on this model indeed show that the FWHM (i.e., BLR size in units of $R_{\rm BLR}/R_{\rm G}$) is governed by the accretion rate $\dot{m}$. Comparison between the model calculations and the observational data of the sample shows that all sources have accretion disks with viscosity α in the range of $0.05 - 1$. It is quite interesting to find that the model calculations can almost reproduce the linear regressions of the correlations (see Figs. 1 and 2), if $\alpha = 0.1$ (or 0.2 for Fig. 2) is adopted in the calculations. This is consistent with the three-dimensional MHD simulations that suggest that the viscosity parameter α in the accretion flows is ~ 0.1 (Armitage 1998), or $\sim 0.05 - 0.2$ (Hawley & Balbus 2002). Our results strongly support the "disk/corona+outflow" model for BLRs suggested by Nicastro (2000).

Acknowledgements We are grateful to D. W. Xu for many helpful discussions and the anonymous referee for valuable suggestions. This work is supported by the National Natural Science Foundation of China for Distinguished Young Scholars (Grant 10325314), and the NSFC Grant 10333020.

References

Antonucci R., 1993, ARA&A, 31, 473
Antonucci R., Miller J. S., 1985, ApJ, 297, 621
Armitage P. J., 1998, ApJ, 501, L189
Chiang J., 2002, ApJ, 572, 79
Gu Q., Huang J., 2002, ApJ, 579, 205
Hawley J. F., Balbus S. A., 2002, ApJ, 573, 738
Hubeny I., Blaes O., Krolik J. H., Agol E., 2001, ApJ, 559, 680
Kaspi S., Smith P. S., Netzer H. et.al., 2000, ApJ, 533, 631
Laor A., 2003, ApJ, 590, 86
Lightman A. P., Eardley D. M., 1974, ApJ, 187, L1
McLure R. J., Jarvis M. J., 2002, MNRAS, 337, 109
Netzer H., 1991, In: T. J. L. Courvoisier, M. Mayor, eds., Active Galactic Nuclei, Berlin: Springer, p.328
Nicastro F., 2000, ApJ, 530, 65
Nicastro F., Martocchia A., Matt G., 2003, ApJ, 589, L13
Peterson B. M., 1993, PASP, 105, 247
Peterson B. M., Barth A. J., Berlind P. et al., 1999, ApJ, 510, 659
Shakura N. I., Sunyaev R. A., 1973, A&A, 24, 337
Shakura N. I., Sunyaev R. A., 1976, MNRAS, 175, 613
Tran H. D., 1995, ApJ, 440, 597
Tran H. D., 2001, ApJ, 554, L19
Tran H. D., 2003, ApJ, 583, 632
Veilleux S., Sanders D. B., Kim D.-C., 1997, ApJ, 484, 92
Veilleux S., Sanders D. B., Kim D.-C., 1999, ApJ, 522, 139
Warner C., Hamann F., Dietrich M., 2004, ApJ, 608, 136
Wei J. Y., Xu D. W., Dong X. Y. et al., 1999, A&AS, 139, 575
Witt H. J., Czerny B., Zycki P. T., 1997, MNRAS, 286, 848
Xu D. W., Komossa S., Wei J. Y. et al., 2003, ApJ, 590, 73